A Mesh Refinement Study on the Impact Response of a Shuttle Leading-Edge Panel Finite Element Simulation

Karen E. Jackson and Edwin L. Fasanella
US Army Research Laboratory, VTD
Hampton, VA

Karen H. Lyle
NASA Langley Research Center
Hampton, VA

Regina L. Spellman
NASA Kennedy Space Center
Cape Canaveral, FL

Abstract

A study was performed to examine the influence of varying mesh density on an LS-DYNA simulation of a rectangular-shaped foam projectile impacting the space shuttle leading edge Panel 6. The shuttle leading-edge panels are fabricated of reinforced carbon-carbon (RCC) material. During the study, nine cases were executed with all possible combinations of coarse, baseline, and fine meshes of the foam and panel. For each simulation, the same material properties and impact conditions were specified and only the mesh density was varied. In the baseline model, the shell elements representing the RCC panel are approximately 0.2-in. on edge, whereas the foam elements are about 0.5-in. on edge. The element nominal edge-length for the baseline panel was halved to create a fine panel (0.1-in. edge length) mesh and doubled to create a coarse panel (0.4-in. edge length) mesh. In addition, the element nominal edge-length of the baseline foam projectile was halved (0.25-in. edge length) to create a fine foam mesh and doubled (1.0-in. edge length) to create a coarse foam mesh. The initial impact velocity of the foam was 775 ft/s. The simulations were executed in LS-DYNA for 6 ms of simulation time. Contour plots of resultant panel displacement and effective stress in the foam were compared at four discrete time intervals. Also, time-history responses of internal and kinetic energy of the panel, kinetic and hourglass energy of the foam, and resultant contact force were plotted to determine the influence of mesh density.

Introduction

Following the Space Shuttle Columbia disaster on February 1, 2003, and during the subsequent investigation by the Columbia Accident Investigation Board (CAIB), various teams from industry, academia, national laboratories, and NASA were requested by Johnson Space Center (JSC) Orbiter Engineering to apply "physics-based" analyses to characterize the expected damage to the shuttle thermal protection system (TPS) tile and Reinforced Carbon-Carbon (RCC) material, for high-speed foam impacts. The forensic evidence from the Columbia debris eventually led investigators to conclude that the breach to the shuttle TPS was caused by a large piece of External Tank (ET) foam that impacted and penetrated the left-wing leading-edge panel, shown in Figure 1. As a result, NASA authorized a series of tests that were performed at Southwest Research Institute to characterize the impact response of the leading-edge RCC panels.

Recommendation 3.3-2 of the CAIB report [1] requests that NASA initiate a program to improve the impact resistance of the wing leading edge. The second part of the recommendation is to "determine the actual impact resistance of current materials and the effect of likely debris strikes." For Return-to-Flight (RTF), a team consisting of personnel from NASA Glenn Research Center, NASA Langley Research Center, and Boeing Philadelphia was given the following task: to develop a validated finite element model of the shuttle wing leading edge

capable of accurately predicting the threshold of damage from debris including foam, ice, and ablators for a variety of impact conditions. Since the CAIB report was released, the team has been developing finite element models of the RCC leading-edge panels; executing the models using LS-DYNA [2]; conducting detailed material characterization tests to obtain dynamic material property data; and, correlating the LS-DYNA analytical results with experimental data obtained from impacts tests onto RCC panels. Some of the early results of this research are described in References 3-7.

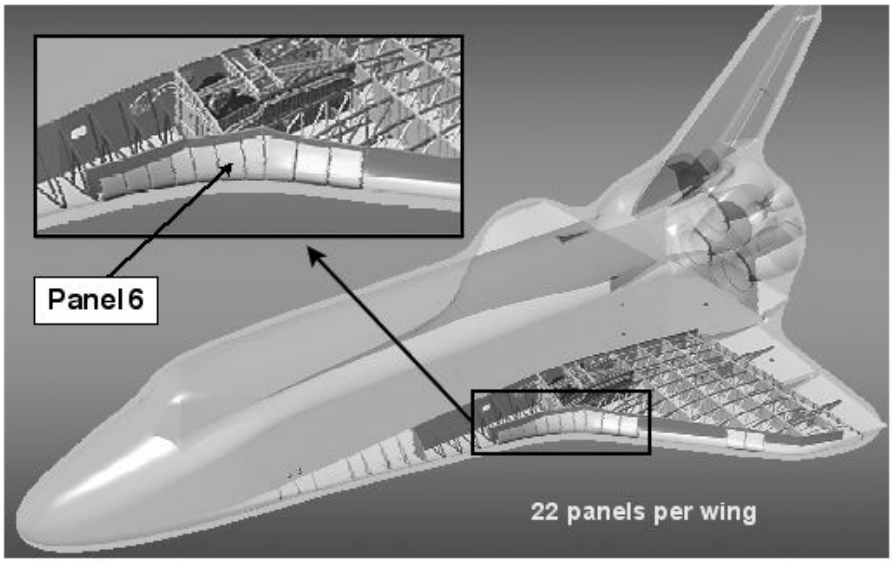

Figure 1. Drawing of the left wing area of the space shuttle.

The purpose of this report is to describe a mesh refinement study that was performed as part of the ongoing RTF modeling efforts. In particular, the mesh study was focused on simulating a rectangular foam projectile, having the same material properties as the BX-250 foam used on the shuttle ET, impacting the shuttle leading-edge RCC Panel 6 at a velocity of 775 ft/s. The location of Panel 6 on the left wing of the shuttle is highlighted in Figure 1. An actual impact test of a BX-250 foam block onto RCC Panel 6 was performed at Southwest Research Institute on June 5, 2003. While the finite element model was originally developed to generate analytical predictions for correlation with experimental data obtained from this test, the focus of the mesh refinement study described in this report is strictly analytical.

For the mesh refinement study, nine cases were executed with all possible combinations of coarse, baseline, and fine meshes of the foam and panel. For each simulation, the same material properties and impact conditions were specified and only the mesh density was varied. The simulations were executed in LS-DYNA for 6 ms of simulation time. Predicted structural deformations and time-history responses are compared for each simulation.

Model Description

The complete model including the foam projectile and the RCC Panel 6 is shown in Figure 2. The Panel 6 model was discretized using Belytachko-Tsay quadrilateral shell elements having nominal element edge lengths of 0.1-, 0.2-, and 0.4-inches for the fine, baseline, and coarse meshes, respectively. A schematic illustrating the different mesh densities for the panel is shown

in Figure 3. The panel model consisted of 19 different parts including the panel midsection, two bottom flanges, two side ribs, two apex ribs, and twelve bolt-holes. These parts are labeled in Figure 4.

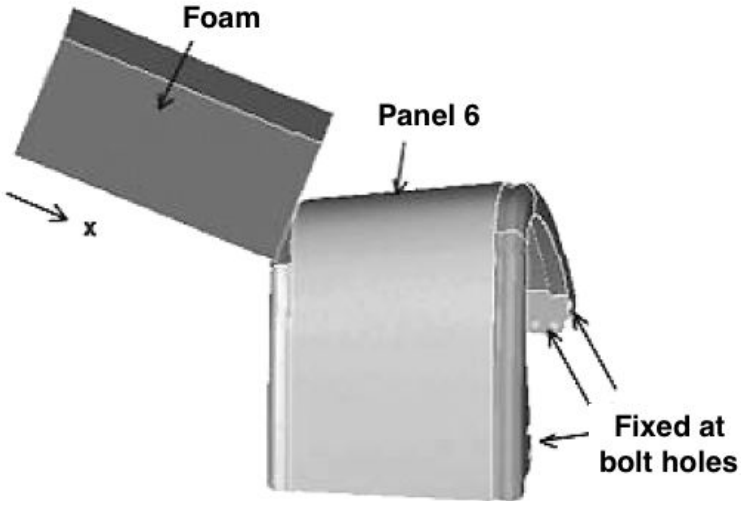

Figure 2. Foam projectile and shuttle RCC Panel 6 model.

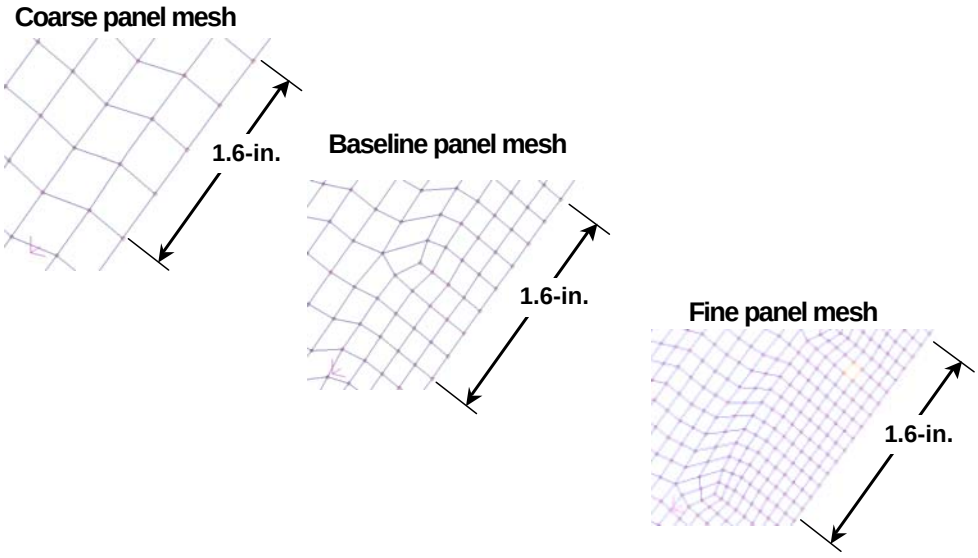

Figure 3. Comparison of Panel 6 mesh densities.

The quadrilateral shell elements representing the RCC panel midsection and ribs were assigned material 58, designated MAT_LAMINATED_COMPOSITE_FABRIC. These parts were modeled as a 19-ply laminated composite fabric with the fibers in each layer oriented in the 0°/90° direction. The bottom flanges were modeled as a 25-ply laminated composite fabric, having slightly different stiffness and strength properties for the RCC material. The rib apex parts were also modeled as a 19-ply laminated composite fabric again having slightly different properties than the RCC material assigned to the midsection and ribs. Three unique material designations were used to specify the material properties of the RCC in the model. These three specifications were needed to account for differences in flight conditioned, mass degraded, and damaged material states.

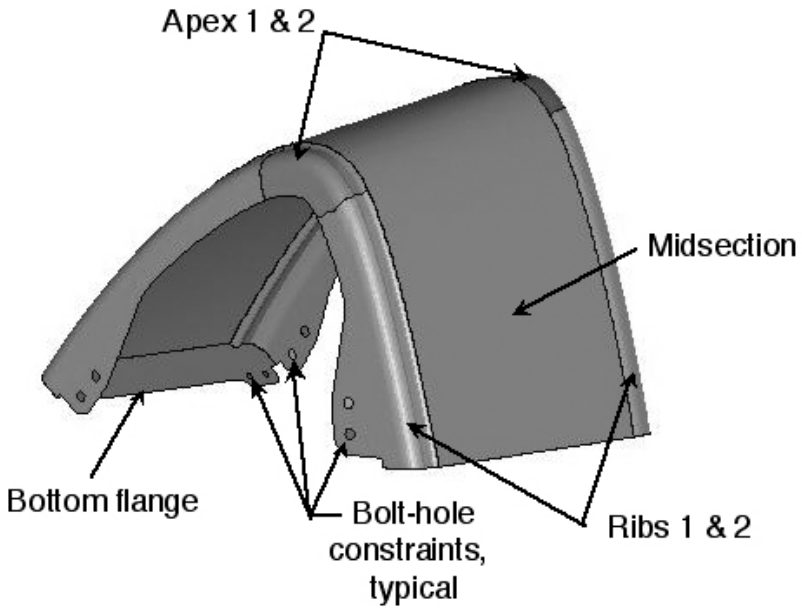

Figure 4. Part designations for the RCC Panel 6 model.

For each RCC material designation, average degraded material properties were used. Prior testing of RCC material shows that it is much stiffer and stronger in compression than in tension, thus requiring a bimodular material model. Also, the stiffness and strength of pristine RCC material are significantly higher than flight-conditioned material. Consequently, the term 'degraded' refers to the fact that flight-conditioned material properties were used. RCC also exhibits considerable variability in material response and it is common to see a band or range of curves used to describe the tensile and/or compressive response, typically maximum, average, and minimum response curves. For this study, the term 'average' means that the average curve was chosen for input.

In the actual RCC Panel 6, bolts were used to support and constrain the panel at the bolt-hole locations. To account for the constraint provided by the bolts in the model, the bolt-holes were represented using 0.1-in.-thick shell elements that were assigned rigid material properties using material 20, designated MAT_RIGID. Then, these elements were constrained from translational motion in the x-, y-, and z-directions using the BOUNDARY_PRESCRIBED_MOTION_RIGID card in LS-DYNA.

The finite element model of the BX-250 foam projectile had overall dimensions of 5.5 x 11.5 x 22.5-in. and was discretized using hexagonal solid elements having nominal element edge lengths of 0.25-, 0.5-, and 1.0-in. for the fine, baseline, and coarse meshes, respectively. A schematic illustrating the different foam mesh densities is shown in Figure 5. Also, a comparison of the total number of nodes and elements in the three foam and three panel meshes is provided in Table 1. The foam block represented a single part in the LS-DYNA model, making the total number of parts in the model equal to 20. The foam block weighed 1.67 lb.

The material properties of the BX-250 foam were represented using material type 83 MAT_FU_CHANG_FOAM with MAT_ADD_EROSION in LS-DYNA. The erosion card is added to allow for element failure in the foam constitutive model. The experimental foam

material responses were input into the model using the DEFINE_CURVE command in LS-DYNA. The responses were obtained from testing of foam components performed at NASA Glenn Research Center. These tests were conducted to determine the influence of strain rate on the compressive response of the foam material. Results for two strain rates, 0.01 s^{-1} and 25 s^{-1}, are plotted in Figure 6. The material response data are plotted only up to 200-psi stress to aid in visualization of the differences caused by strain rate; however, the stress data at strain values approaching 1 are 70,000 psi and higher. The response of the BX-250 foam, shown in Figure 6, is typical of other foam responses in that it exhibits a linear response at low strains, and as crushing begins a "knee" occurs in the response. Then, as stable crushing continues, the stress increases gradually until the cells within the foam begin to compact. As compaction initiates and continues, the stress increases dramatically for relatively small increases in strain. As shown in Figure 6, the influence of strain rate is to increase the stress at which the knee occurs, to increase the stress during stable crushing, and to lower the strain at which compaction begins. A tensile failure stress of 65-psi was assigned to the foam.

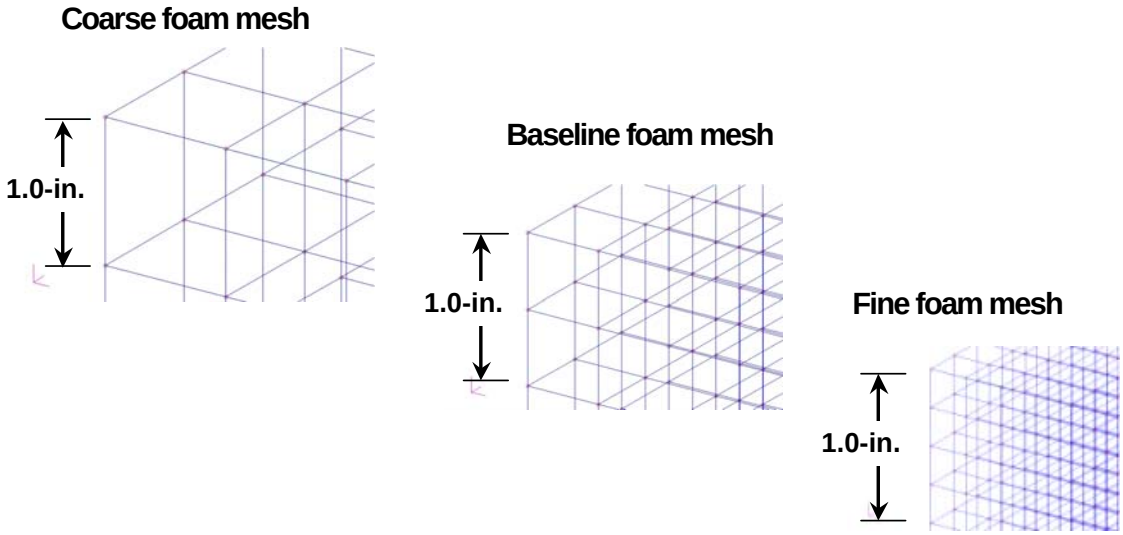

Figure 5. Comparison of mesh densities used for the foam.

Table 1. Comparison of the number of elements and nodes per panel and foam mesh.

Mesh density	Panel		Foam	
	Number of elements	Number of nodes	Number of elements	Number of nodes
Coarse	11,170	11,459	1,380	1,872
Baseline	32,109	32,432	11,385	13,248
Fine	128,172	141,723	92,092	99,452

All of the nodes used to create the foam projectile were assigned an initial velocity of 775 ft/s (9,300 in/s) in the x-direction, which is defined along the long edge of the foam block (see Figure 2). A CONTACT_ERODING_NODES_TO_SURFACE was specified between the panel midsection and the foam in the model. For this contact, the panel midsection was designated the master surface, and the foam was the slave. Due to the eroding feature of this contact definition, a foam element may fail, or erode, and the contact will be picked up by the next element.

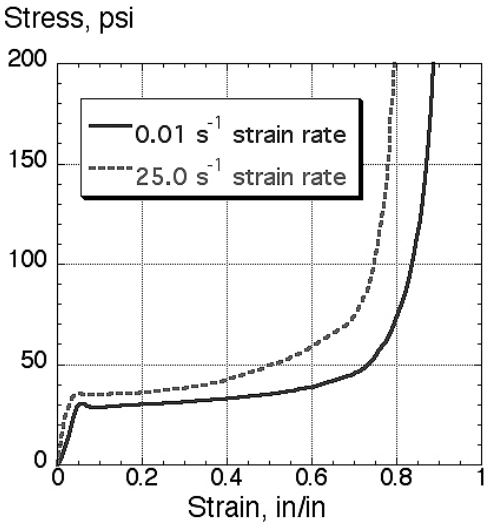

Figure 6. Compressive material properties of BX-250 foam for two different strain rates.

For this analytical study, nine simulations were performed for every combination of coarse, baseline, and fine mesh of the foam and RCC Panel 6. The matrix of simulations and the naming scheme used to differentiate the models are shown in Figure 7. For these nine simulations, the same material properties were used for the foam and panel and the same initial velocity and contact definitions were specified. Only the mesh densities were varied. Each model was executed for 0.006 s (6 ms) of simulation time using LS-DYNA Version 960. The simulations were run on a single-processor Linux-based Hewlett Packard workstation x4000.

Simulation Results

The results of the analytical study are presented as contour or fringe plots of resultant panel deflections, contour plots of effective stress in the foam, and time-history plots of internal and kinetic energy of the panel midsection, the resultant contact force response, and the kinetic and hourglass energy of the foam.

Contour Plots of Predicted Resultant Panel Deflections

The predicted resultant panel deflections are shown in Figures 8 through 11 at discrete time intervals of 2.8, 3.8, 5.0, and 6.0 ms, respectively. The results are shown using the format illustrated in Figure 7, and the maximum deflection values are provided in the parenthesis beneath each contour plot at each time interval. Note that the contour plots are shown for the same fringe levels at each time interval; however, the maximum value of the range is different for each time interval. To orient the reader, the contour plots shown in Figures 8-11 were created by turning the panel on its edge and viewing the lower surface of the panel midsection through the bottom flanges.

At 2.8-ms, the trend is that, for a constant panel mesh, increases in foam mesh density cause a decrease in maximum deflection. However, for a constant foam mesh, increases in panel mesh density produce an increase in maximum deflection. Given this trend, the fine panel:coarse foam (FP:CF) model exhibits the maximum deflection of all the combinations of foam and panel meshes for this time intervals. No failure of the panel has occurred by 2.8 ms, as shown in Figure 8.

Coarse Panel:Coarse Foam (CP:CF)	Coarse Panel:Baseline Foam (CP:BF)	Coarse Panel:Fine Foam (CP:FF)
Baseline Panel:Coarse Foam (BP:CF)	Baseline Panel:Baseline Foam (BP:BF)	Baseline Panel:Fine Foam (BP:FF)
Fine Panel:Coarse Foam (FP:CF)	Fine Panel:Baseline Foam (FP:BF)	Fine Panel:Fine Foam (FP:FF)

Figure 7. Analysis matrix.

By 5.0 ms, all of the panels have failed with cracking of the rib area as a common damage mode, as seen in Figure 11. In all but two cases, the rib cracks initiate at the interface region between the rib and apex, where the material properties change. The two exceptions are the baseline panel:baseline foam (BP:BF) and the baseline panel:fine foam (BP:FF). For these two models, the crack initiates in the rib area only, away from the rib/apex interface. The rib crack is the only damage seen in the coarse and baseline panels at this time step. In comparison, the rib crack in the fine panel models has grown downward, separating a portion of the rib from the panel. By 5.0 ms, the panel midsection has failed in all of the fine panel models. The panel failure is characterized by the formation of a large crack in the panel midsection that runs parallel to the rib/panel interface. Finally, the FP:FF model exhibits a second crack in the panel midsection that runs normal to the rib/panel interface. A similar crack is not observed in the fine panel models with coarse or baseline foam meshes.

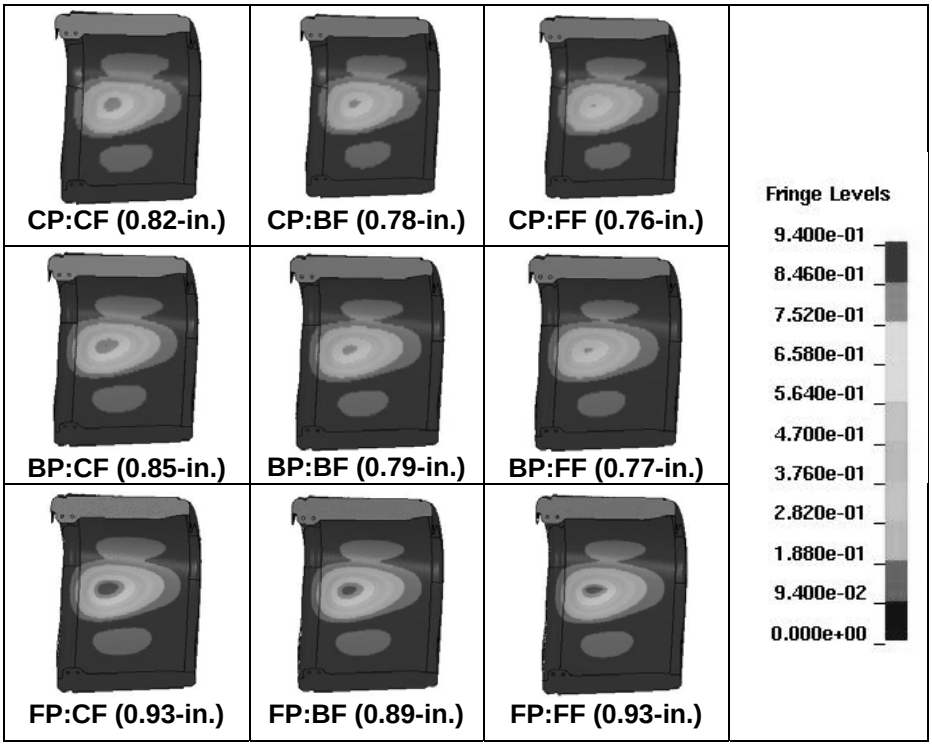

Figure 8. Resultant deflection plots of RCC Panel 6 at 2.8 ms.

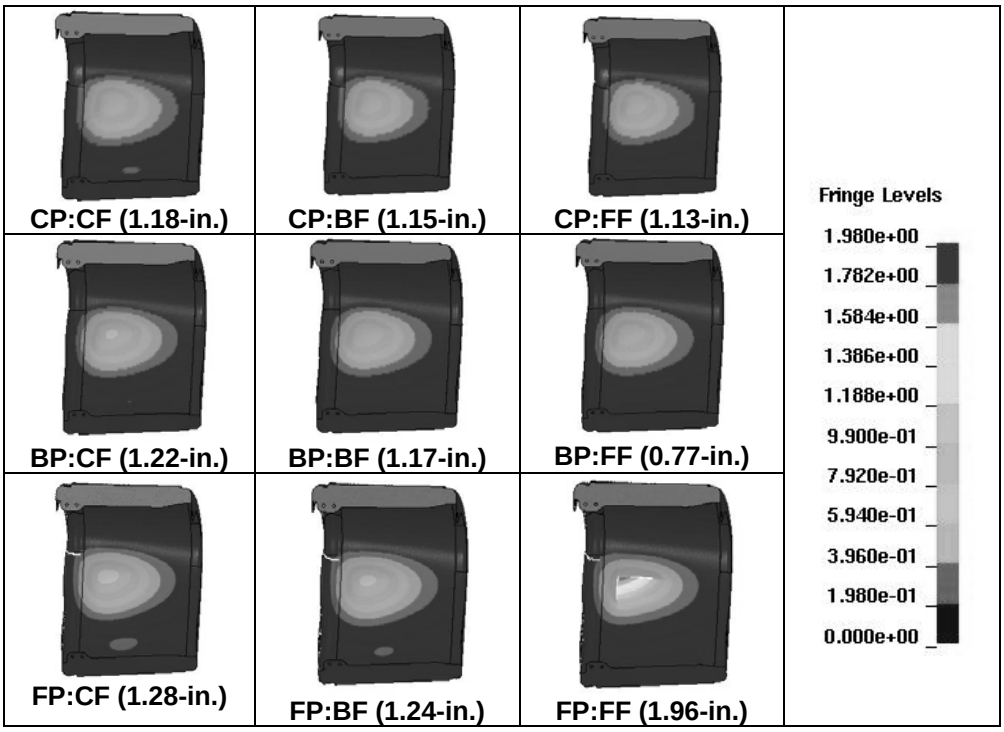

Figure 9. Resultant deflection plots of RCC Panel 6 at 3.8 ms.

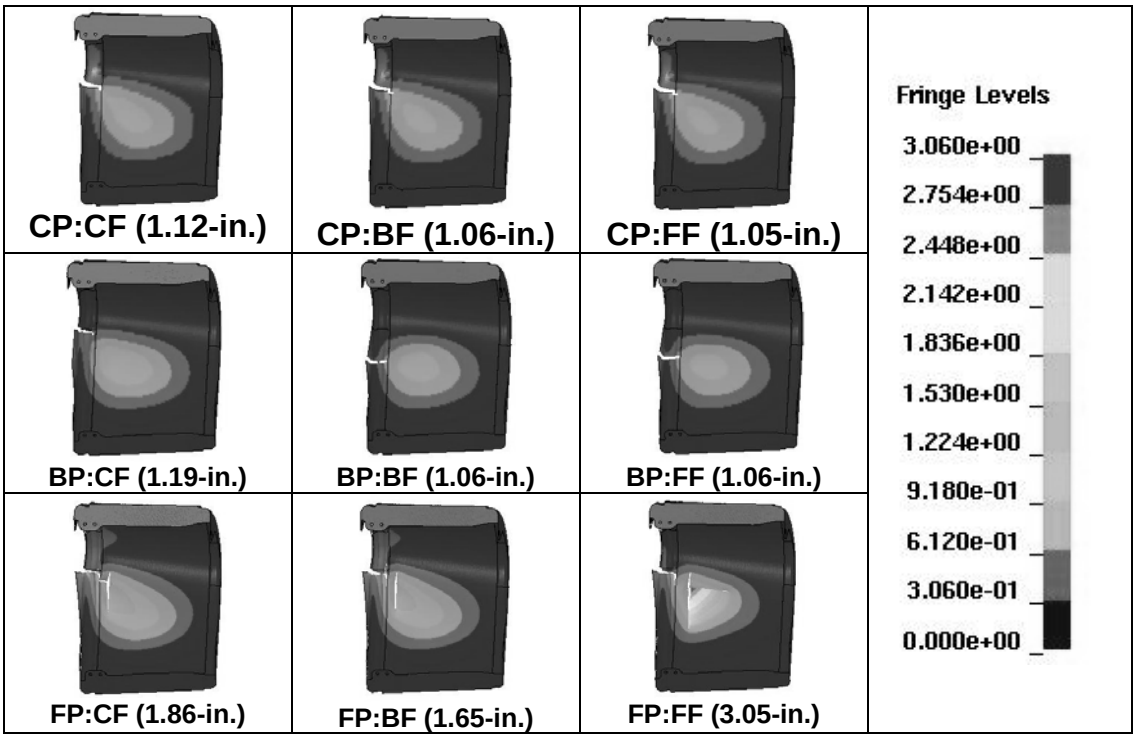

Figure 10. Resultant deflection plots of RCC Panel 6 at 5.0 ms.

By 6.0 ms, the rib/apex cracks in all of the coarse panel models and in the BP:CF model have grown downward along the rib/panel interface, as shown in Figure 12. The rib cracks in the baseline panel models with baseline and fine foam are stable, exhibiting no increase in the crack size or formation of new damage. The damage in the fine panel models is also stabilized.

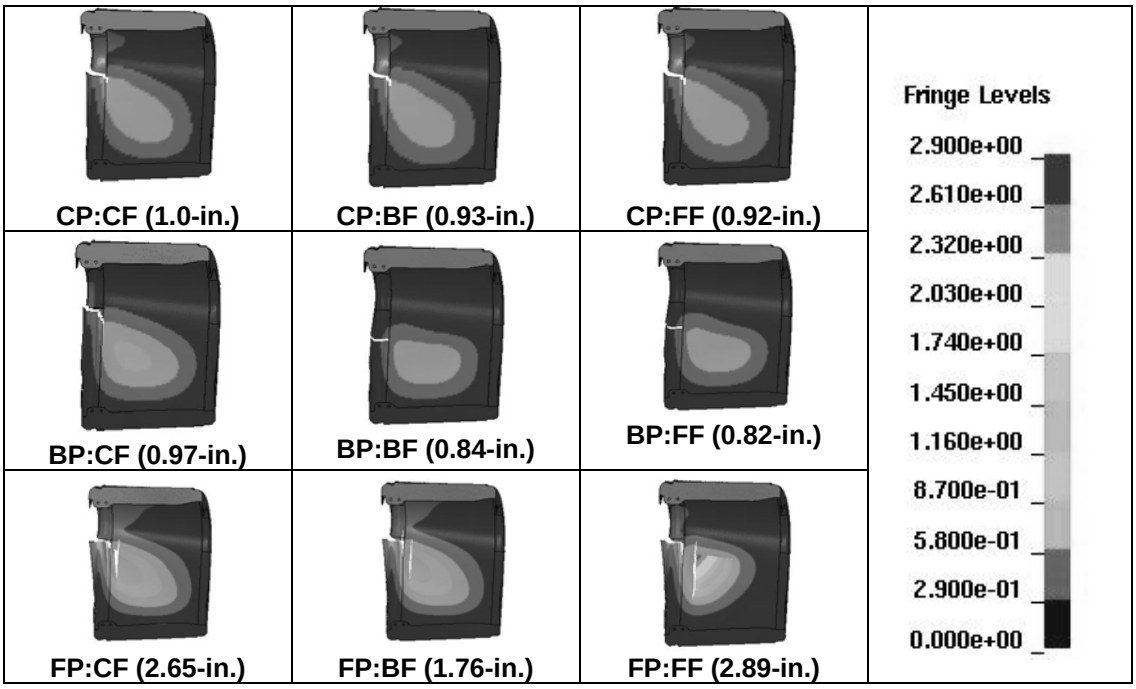

Figure 11. Resultant deflection plots of RCC Panel 6 at 6.0 ms.

Contour Plots of Predicted Effective Stress in the Foam Projectile

Contour plots of effective stress for varying foam densities are shown in Figures 12-14, for constant coarse, baseline, and fine panel meshes, respectively. Note that the same fringe levels are used in each figure. The plots show that the amount of damage in the foam increases as the mesh density of the foam increases, for a constant panel mesh. Thus, the fine foam model exhibits the maximum damage in each case. This trend is observed for all panel meshes.

Time-History Response Comparisons

Comparisons of predicted time-history responses for internal and kinetic energy of the panel, kinetic and hourglass energy of the foam, and resultant contact force are shown in Figures 15-17 for coarse, baseline, and fine panel meshes with varying foam meshes, respectively.

The time-history results for the coarse panel with varying foam meshes are shown in Figure 15. The internal and kinetic energy responses of the panel and the kinetic energy responses of the foam show only minor differences due to varying foam mesh densities. No differences in the overall magnitude and duration of the resultant contact force time-history are seen, as shown in Figure 15 (d); however, the coarse foam response contains high-frequency oscillations, while the baseline and fine foam responses are smooth. As seen in Figure 15 (e), the coarse foam response exhibits significantly higher hourglass energy that the baseline or fine foam responses. Generally, this finding would make the coarse foam mesh undesirable; however, the magnitude of the hourglass energy is small when compared with the kinetic energy of the foam.

Similar trends are observed in the time-history responses of the baseline panel with varying foam mesh densities, plotted in Figure 16. The primary difference between the coarse and baseline panel responses is that the hourglass energy of the coarse foam curve is lower for the baseline

case. However, the amount of hourglass energy in the coarse foam is still greater than that in the baseline or fine foam.

Time, ms	Coarse Foam	Baseline Foam	Fine Foam	Fringe Info
2.8	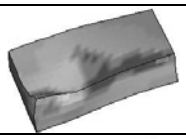	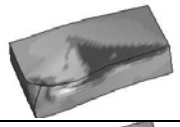	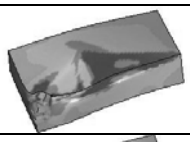	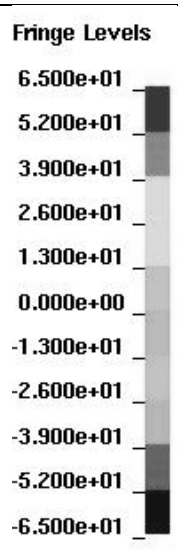
3.8	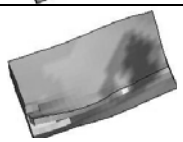	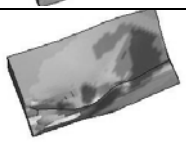	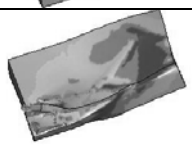	
5.0		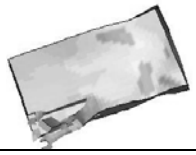		
6.0	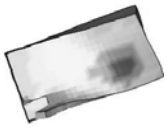		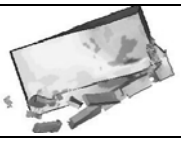	

Figure 12. Effective stress fringe plots for varying foam densities and a coarse panel mesh.

Time, ms	Coarse Foam	Baseline Foam	Fine Foam	Fringe Info
2.8	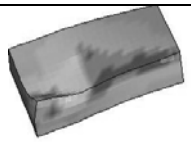	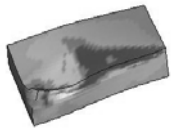	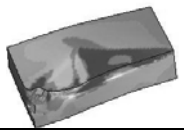	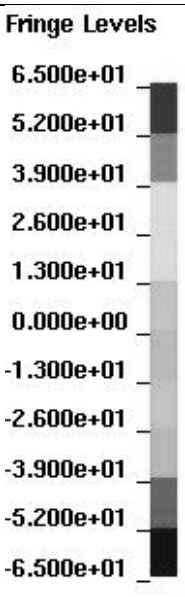
3.8	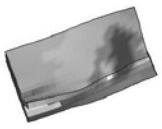	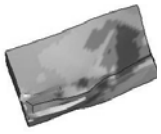	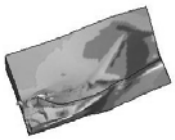	
5.0			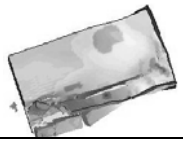	
6.0	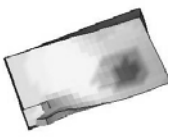	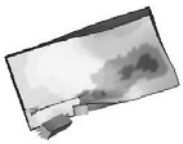		

Figure 13. Effective stress fringe plots for varying foam mesh densities and a baseline panel.

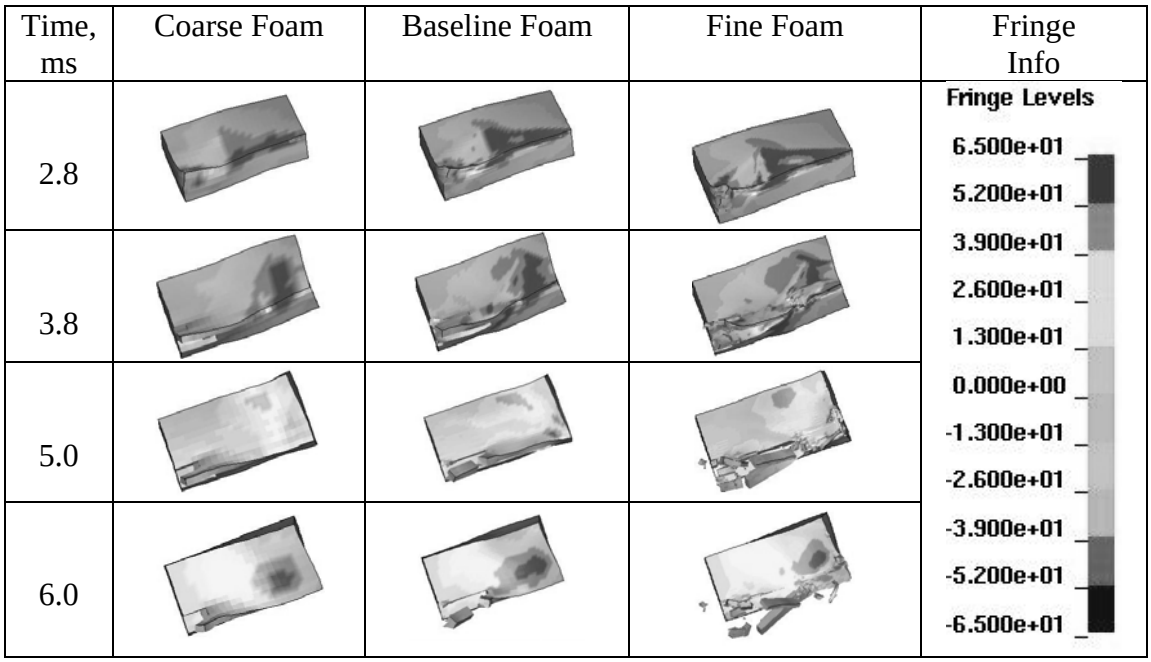

Figure 14. Effective stress fringe plots for varying foam mesh densities and a fine panel mesh.

The time-history responses for the fine panel with varying foam mesh densities are shown in Figure 17. Unlike the coarse and baseline panels where only minor differences were seen in the internal and kinetic energy responses of the panel as a function of varying foam mesh density, the fine panel results show much larger variations in these responses, as shown in Figures 17 (a) and (b). In both cases, the FP:CF model exhibits the highest magnitude response. However, only minor differences in the kinetic energy responses of the foam, shown in Figure 17 (c), are observed for the differing foam mesh densities. The resultant contact force responses are of equal magnitude and duration, see Figure 17 (d), and the coarse foam response exhibits high-frequency oscillations, not seen in the other responses. The large spike in the fine foam response is attributed to instabilities in the contact algorithm. Finally, the hourglass energy responses are shown in Figure 17 (e), with the coarse foam response exhibiting the highest amount of hourglass energy. However, even for the coarse mesh, the magnitude of the hourglass energy is only a fraction of the kinetic energy of the foam.

Discussion of Results

An important factor for consideration in this study is the computational expense required to run the fine foam and fine panel models. The time step used in executing the model is equal to the time it takes a sound wave to cross some characteristic length, which is a function of the smallest element in the model. Thus, the finer the mesh, the smaller the time step. For example, the initial time step for the CP:CF model was 2.9E-7 s and the time step for the FP:FF model was 1.4E-7 s. These two models required 4 and 101 hours of CPU for execution, respectively. For comparison, the BP:BF model had an initial time step of 2.7E-7 s and required 14 hours of CPU. The baseline mesh discretization is a good choice for future simulations in that it captures the structural behavior and damage progression of the panel and foam without the computational expense of the fine mesh discretization. As shown in Figures 15-17, the coarse foam mesh should be avoided due to the high levels of hourglass energy in the model.

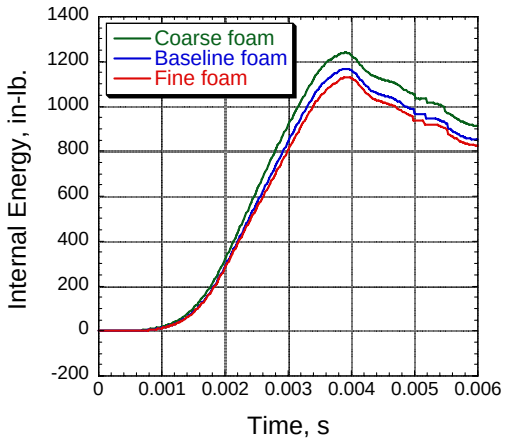

(a) Internal energy of the panel.

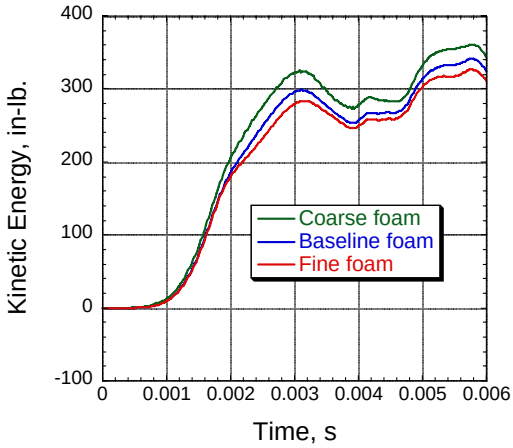

(b) Kinetic energy of the panel.

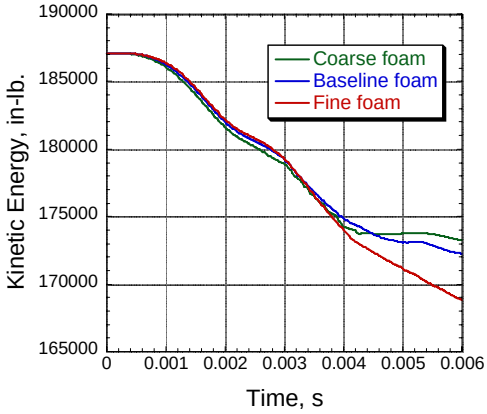

(c) Kinetic energy of the foam.

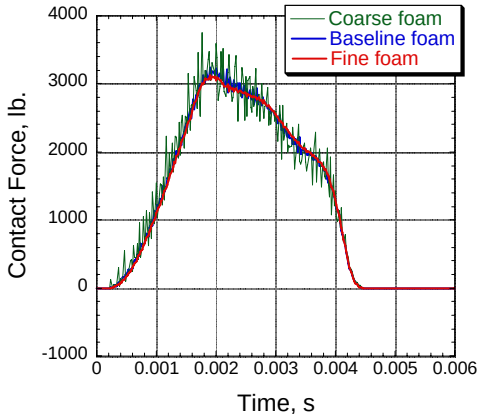

(d) Contact force.

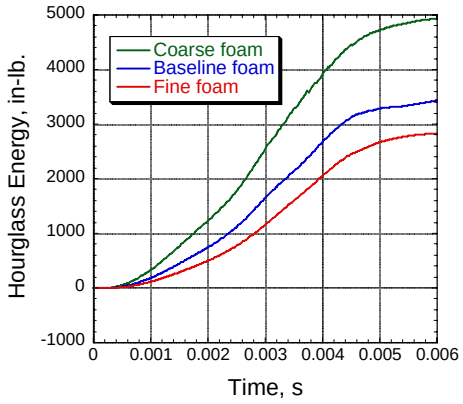

(e) Hourglass energy of the foam.

Figure 15. Predicted time-history responses for a constant coarse panel mesh and varying foam densities.

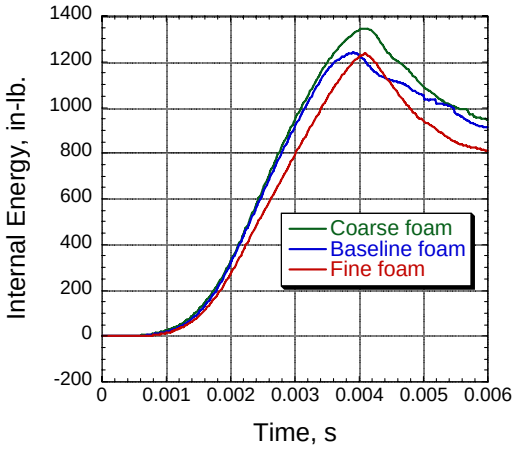

(a) Internal energy of the panel.

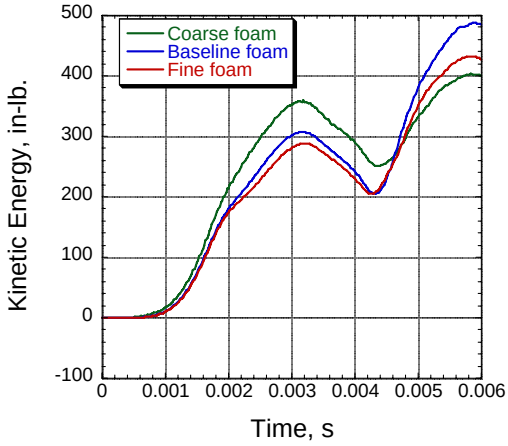

(b) Kinetic energy of the panel.

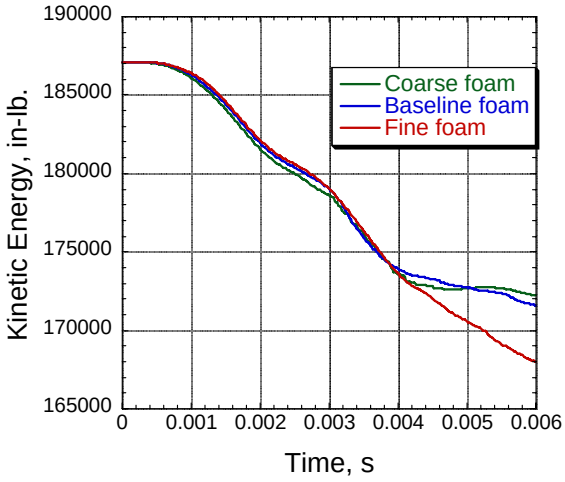

(c) Kinetic energy of the foam.

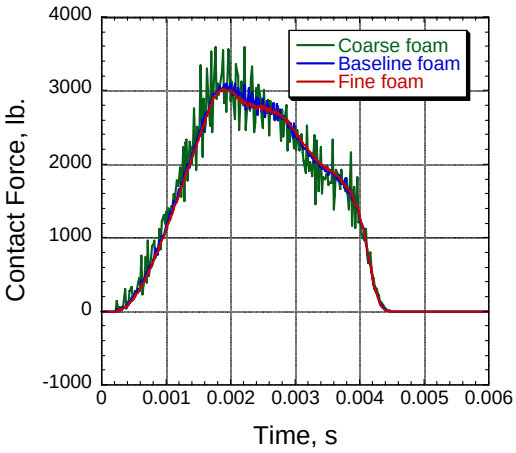

(d) Contact force.

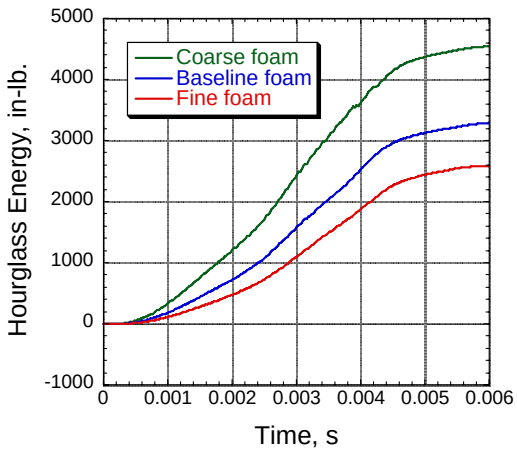

(e) Hourglass energy of the foam.

Figure 16. Predicted time-history responses for a constant baseline panel mesh and varying foam densities.

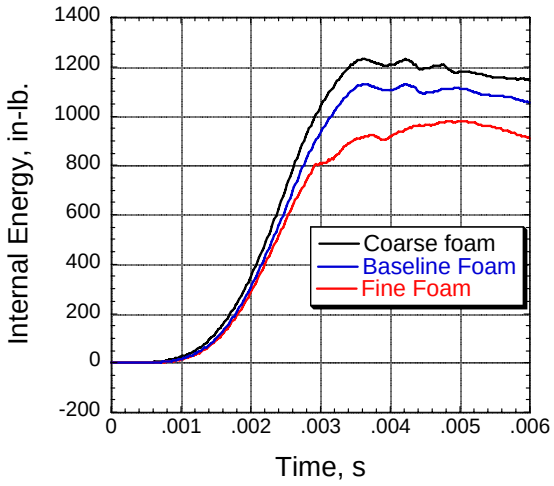

(a) Internal energy of the panel.

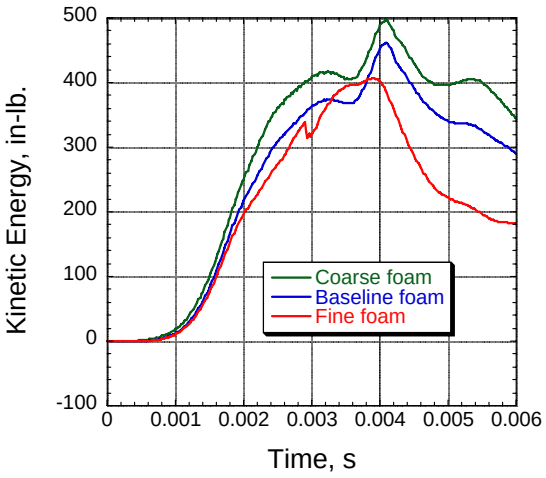

(b) Kinetic energy of the panel.

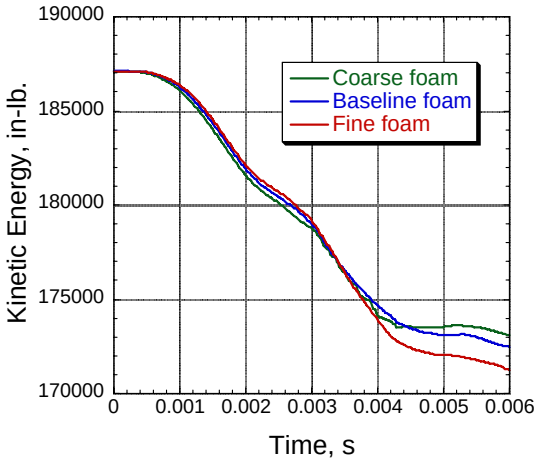

(c) Kinetic energy of the foam.

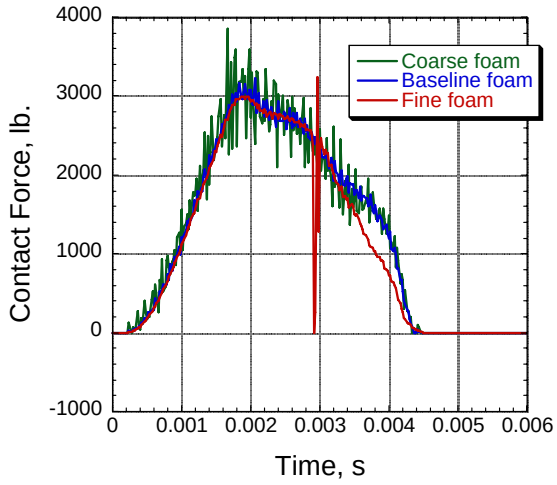

(d) Contact force.

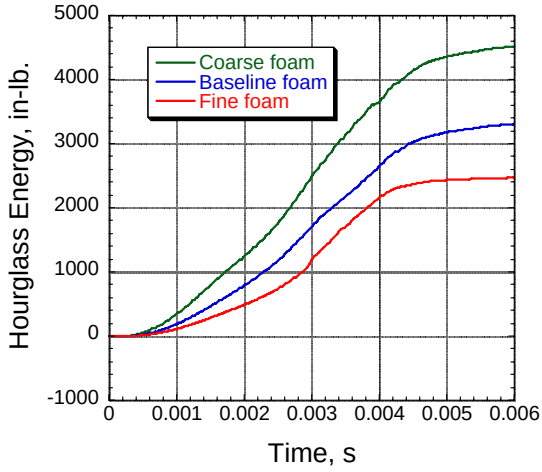

(e) Hourglass energy of the foam.

Figure 17. Predicted time-history responses with a constant fine panel mesh and varying foam densities.

Concluding Remarks

A mesh density study was performed in support of the Shuttle Return-To-Flight program based on an LS-DYNA simulation of a foam projectile impacting one of the reinforced carbon-carbon (RCC) leading edge panels on the space shuttle (Panel 6). For the study, three meshes (coarse, baseline, and fine) were used for the foam and the panel. Thus, nine simulations were executed representing all possible combinations of foam and panel meshes. For each simulation, the same material properties and impact conditions were specified and only the mesh density was varied. Comparisons of fringe plots of resultant panel displacement and effective stress in the projectile were made for four discrete time intervals. Also, time-history responses of internal and kinetic energy of the panel, kinetic and hourglass energy of the foam, and the resultant contact force were plotted to determine the influence of mesh density.

The findings from this study are summarized, as follows. Before failure, the trend is that increasing panel mesh density results in increasing maximum deflection for a constant foam discretization. However, the opposite is true for increasing foam mesh density, which results in lower maximum deflections for a constant panel discretization. For any foam mesh, the fine panel fails by 3.8 ms, with the FP:FF model exhibiting the largest amount of damage, i.e. panel failure followed by rib cracking. By 5.0 ms, all panels have failed, with rib cracking as the common failure mode. In all but two cases, the rib cracks initiate at the interface region between the rib and apex, where the material properties change. The two exceptions are the BP:BF and the BP:FF models. For these models, the crack initiates in the rib area only, away from the rib/apex interface. For a constant panel mesh, changes in the foam mesh do not substantially affect the internal and kinetic energy time-history results; however, in all cases, the hourglass energy of the foam is highest for the coarse mesh and lowest for the fine mesh. The magnitude and duration of the contact force time-histories for all cases were nearly identical; however, the contact responses of the coarse foam models generally exhibited high-frequency oscillations and the contact responses of the FP:FF models contained large spikes that were attributed to instabilities in the contact algorithm. The baseline mesh discretization is a good choice for future simulations in that it captures the structural behavior and damage progression of the panel and foam without the computational expense of the fine mesh discretization. The coarse foam mesh should be avoided due to the high levels of hourglass energy in the model.

References

1. Gehman, H. W., et al, “Columbia Accident Investigation Board,” Report Volume 1, U. S. Government Printing Office, Washington, DC, August 2003.
2. Anon., “LS-DYNA Keyword User’s Manual Volume I and II – Version 960,” Livermore Software Technology Company, Livermore, CA, March 2001.
3. Carney, K., et al, “Material Modeling of Space Shuttle Leading Edge and External Tank Materials for Use in the Columbia Accident Investigation.” 8th LS-DYNA User’s Conference, Dearborn, MI, May 2-4, 2004.
4. Melis, M.,et al, “A Summery of the Space Shuttle Columbia Tragedy and the Use of LS-DYNA in the Accident Investigation and Return to Flight Efforts,” 8th LS-DYNA User’s Conference, Dearborn, MI, May 2-4, 2004.
5. Gabrys, J., et al, “The Use of LS-DYNA in the Columbia Accident Investigation,” 8th International LS-DYNA User’s Conference, Dearborn, MI, May 2-4, 2004.
6. Lyle, K., et al, “Application of Non-Deterministic Methods to Assess Modeling Uncertainties for Reinforced Carbon-Carbon Debis Impacts,” 8th International LS-DYNA User’s Conference, Dearborn, MI, May 2-4, 2004.
7. Fasanella, E. L., et al, “Test and Analysis Correlation of Foam Impact onto Space Shuttle Wing Leading Edge RCC Panel 8,” 8th International LS-DYNA User’s Conference, Dearborn, MI, May 2-4, 2004.